Reaction Path of a sub-200 fs Photochemical Electrocyclic Reaction

M. Garavelli,[†] C. S. Page,[‡] P. Celani,[†,⊥] M. Olivucci,*[,‡] W. E. Schmid,[||] S. A. Trushin,[§,||] and W. Fuss*[,||]

Dipartimento Chimico "G. Ciamician", Università di Bologna, Via Selmi 2, I-40126 Bologna, Italy, Dipartimento di Chimica, Università di Siena, via Aldo Moro, I-53100 Siena, Italy, B. I. Stepanov Institute of Physics, Belarus Academy of Sciences, 220602 Minsk, Belarus, and Max-Planck-Institut für Quantenoptik, D-85740 Garching, Germany

Received: January 29, 2001

Ab initio multistate second-order perturbation theory (MS−CASPT2) calculations are used to map the reaction path for the ultrafast photochemical electrocyclic ring-opening of cyclohexa-1,3-diene (CHD). This path is characterized by evolution along a complex reaction coordinate extending over two barrierless excited state potential energy surfaces and ultimately leading to deactivation through a S_1/S_0 conical intersection. The observed excited-state dynamics involve three sequential phases with lifetimes (traveling times) of 10, 43, and 77 fs, respectively. In this work we associate each phase to the evolution of the CHD molecular structure along a different mode. In particular, we show that (a) the decay of CHD from its spectroscopic ($1B_2$) state to a lower lying dark ($2A_1$) excited state involves motion along a highly curved coordinate corresponding to a mixture of σ bond expansion and symmetry breaking skeletal bending, (b) the evolution on the $2A_1$ (S_1) state and the final $2A_1 \rightarrow 1A_1$ (i.e., $S_1 \rightarrow S_0$) decay involve a large amplitude displacement along the same asymmetric bending mode which ultimately leads to a S_1/S_0 conical intersection, and (c) the application of a novel strategy for mapping the multidimensional S_1/S_0 intersection space indicates that the ultrashort 77 fs lifetime of the $2A_1$ excited state is due to the existence of an extensive set of S_1/S_0 conical intersection points spanning the low-lying part of the $2A_1$ energy surface. Points (a) and (b) are validated by discussing the results of previously reported and new femtosecond time-resolved spectroscopic data on CHD and on the two dialkyl derivatives α-terpinene and α-phellandrene. An interpretation in terms of driving forces is also given.

1. Introduction

The Woodward−Hoffmann (WH) rules for a photochemical pericyclic reaction typically correlate the first excited state of the reactant with the first excited state of the product and the ground state of the reactant with a doubly excited state of the product, and vice versa. An avoided crossing between the latter two correlation lines gives rise to a collection well (the "pericyclic minimum") in the first excited state. The corresponding diagram is shown in Figure 1 (full line) for the ring opening of 1,3-cyclohexadiene (CHD), a molecule with a C_2 symmetric (half-chair) structure and with singly excited, doubly excited, and ground states of $1B_2$, $2A_1$, and $1A_1$ symmetry, respectively. The diagram exemplifies the reaction path model of van der Lugt−Oosterhoff[1] for a textbook "excited-state allowed reaction".[2] A paradigm of the van der Lugt and Oosterhoff model is that facile $2A_1 \rightarrow 1A_1$ decay occurs in correspondence of the pericyclic minimum. This leads to the concept of "photochemical funnel" which forms the basis of modern mechanistic photochemistry.

In the van der Lugt−Oosterhoff model, it is postulated that the reaction coordinate maintains C_2 symmetry. However, modern quantum chemical work[3] indicates that the minimum energy path departing from the Franck−Condon (FC) structure of CHD has a much more complex reaction coordinate. Such a coordinate ultimately involves a symmetry-breaking deformation of CHD, which leads to an asymmetric S_1/S_0 conical intersection (CI).[4,5,6] This CI corresponds to the reaction photochemical funnel and replaces the concept of pericyclic minimum.

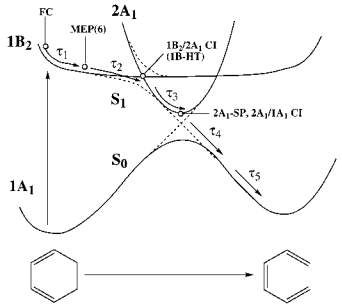

Figure 1. Van der Lugt-Oosterhoff type diagram for the photochemical ring-opening of 1,3-cyclohexadiene (solid lines). The dashed lines represent the computed crossing of the $1B_2$ and $2A_1$ (this work) and $2A_1$ and $1A_1$ surfaces (avoided crossing $1B_2/2A_1$ and conical intersection $2A_1/1A_1$ CI, both lying outside of the drawing plane and along a symmetry-breaking mode. See text for further discussion). The τ_i are experimentally determined time constants (see below). The labels refer to structures computed at the CASSCF level of theory (see text).

After photoexcitation to the bright state ($1B_2$) surface, the molecule is accelerated along a totally symmetric double bond

* To whom correspondence should be addressed.
[†] Dipartimento Chimico "G. Ciamician".
[‡] Dipartimento di Chimica, Università di Siena.
[§] B. I. Stepanov Institute of Physics.
[||] Max-Planck-Institut für Quantenoptik.
[⊥] Present address: Institut für Theoretische Chemie, Universität Stuttgart, Pfaffenwaldring 55, D-70569 Stuttgart, Germany.

10.1021/jp010359p CCC: $20.00
Published on Web 04/14/2001

expansion mode; thereafter, the relaxation becomes dominated by σ bond expansion.[6] Along this coordinate, the system approaches the region of a $1B_2/2A_1$ conical intersection[7] of C_2 symmetry ($1B_2/2A_1$ CI), where relaxation to a lower lying dark state ($2A_1$) may occur. The following relaxation along the $2A_1$ energy surface occurs along a symmetry-breaking coordinate[4,5] down to an energy minimum located on a shallow plateau. The final decay to S_0 occurs via a further distortion of the molecule toward an asymmetric $2A_1/1A_1$ CI (i.e., the S_1/S_0 conical intersection) located on the same plateau.[5a] This scheme has been shown to be common to other hydrocarbons such as *all-trans*-hexa-1,3,5-triene.[5b]

Recent measurements of CHD dynamics by ultrafast spectroscopy with nonresonant ionization[8,9] suggest a correlation between the computed changes in the excited-state reaction coordinate and the observed times. In particular, the initial relaxation (Phase 1), which occurs in 10 fs (τ_1 in Figure 1), may be associated with the initial double bond expansion in the CHD ring. The subsequent step (Phase 2), taking 43 fs (τ_2), is associated with the σ bond expansion leading to the decay of the $1B_2$ species.[6,9] The final stage (Phase 3) involves the evolution on the $2A_1$ surface and the decay to the $1A_1$ ground state. This phase should be associated with the large symmetry-breaking change leading to the asymmetric $2A_1/1A_1$ CI. However, this phase lasts only 77 fs (τ_3), a time that appears unexpectedly short compared with the time scale of hundreds of femtoseconds observed in similar systems[5b] and also surprising in view of the very flat $2A_1$ plateau near this CI.[5a] Two hypotheses can be invoked to account for such an ultrafast process. (1) Upon $1B_2 \rightarrow 2A_1$ decay the system is directly accelerated toward a $2A_1/1A_1$ conical intersection which does not lie along the previously reported $2A_1$ relaxation path (this is a minimum energy path connecting the $1B_2/2A_1$ CI to the $2A_1$ energy minimum). (2) The probability of hitting a conical intersection during motion along the bottom of the $2A_1$ energy surface is much higher than expected due to the existence of a large set of conical intersection point spanning the lower lying region of the surface.

In the present work we investigate the mechanistic hypotheses (1)−(2) using energy surface mapping and ab initio multistate second-order perturbation theory (MS−CASPT2) computations. In particular, we show that the use of a novel strategy designed to map the low-lying region of the $2A_1/1A_1$ intersection space provides an explanation for the ultrashort lifetime of the $2A_1$ species. In fact, our results indicate the existence of an extended set of CI points with energies slightly higher than that of the previously computed $2A_1/1A_1$ CI,[5a] which supports hypothesis 2. Furthermore, as a confirmation of our general mechanistic picture of the CHD ring-opening, we present new experimental data on the CHD derivatives α-terpinene and α-phellandrene that validate the computed reaction coordinate changes during the initial 10 and 43 fs phases.

2. Methods

2.1. Computations. All of the energy, gradient, and frequency computations presented in this work have been carried out at the ab initio complete active space (CASSCF) level of theory, with the double-ζ + polarization (6-31G*) basis sets available in *Gaussian 94*.[10] The S_1 minima, transition states and MEPs have been computed using an active space of 6 electrons in 6 orbitals (i.e., the four valence π and the two valence σ orbitals involved in the ring-opening of CHD). In order to improve the energetics by including the effect of dynamic electron correlation, the energies of selected points were recomputed at the multiconfigurational and multistate second-order perturbation theory levels using the CASPT2 and MS−CASPT2 methods[11] implemented in the *MOLCAS 4* series of programs.[12]

The vibrational frequencies of stationary (energy minima and transition structures) and nonstationary points (i.e., points on the minimum energy path, MEP) were computed analytically using the methods available in *Gaussian 94*.[10] The calculated frequency values were all scaled uniformly by a factor of 0.9, as is usual for the methods employed. In the case of nonstationary points (i.e., points with a nonzero energy gradient, such as the Franck−Condon point) the computed Hessian was projected onto the $(f - 1)$-dimensional space orthogonal to the energy gradient. The diagonalization of this projected Hessian yielded the $(f - 1)$ normal modes and frequencies.[13,14] These were used to determine the shape (e.g., valley-like or ridge-like) of the S_1 surface along the computed MEP.

In the present work, we characterize the conical intersections $1B_2/2A_1$ and $2A_1/1A_1$ associated with the population and decay of the $2A_1$ state. Furthermore, we describe the low-lying part of the $2A_1/1A_1$ intersection space. Accordingly, we have devised a new computational strategy capable of locating *steepest descent paths within an intersection space*. This is based on a combination of the recently introduced IRD (intrinsic relaxation direction) method for finding local steepest descent directions from a nonstationary point[15a] and the standard CIO (conical-intersection optimization) method for locating conical intersections[15b] as stationary points within the intersection space. The details of this methodology are given in the appendix.

2.2. Experimental Procedure. The molecules were pumped in the gas phase by a frequency-tripled pulse of a Ti-sapphire laser system (267 nm, 130 fs) and then probed by nonresonant multiphoton dissociative ionization at the fundamental wavelength (800 nm, 110 fs, 2×10^{13} W cm^{-2}). As with transient absorption, this method is based on the probing of electronic transitions; both can give information (mainly lifetimes) on specific locations on the potential energy surface (PES). However, transient dissociative ionization reveals more detail, permitting one to monitor the evolution of the molecules all the way down the PES. Furthermore, it yields an effective time resolution below the pulse lengths.[16] Both advantages result from the fact that quite a number of time-dependent ion signals (parent and fragments) are found which are linearly independent.[9]

For evaluation, we assume that the molecule sequentially reaches several locations i (observation windows) on the potential energy surfaces with lifetime τ_i, and the temporal evolution is simulated by rate equations. Since these times turn out to be very short (<100 fs), the transit time through the window makes a significant contribution to τ_i. Therefore, we use the terms "lifetime" (time constant) and "traveling (transit) time" interchangeably. The signals are then expressed as a sum of exponentials (with time constants τ_i) convoluted with the (Gaussian) pump and probe pulses. They result from linear combinations of the time-dependent populations of each window, the coefficients being the cross sections ${}^M\sigma_i$, to produce an ion of mass M from window i. The time constants τ_i are determined in two ways: (1) the longer ones ($\tau_i > 30$ fs; i.e., τ_2 and τ_3) from a single exponential fit to the decay of the signal and (2) the shorter ones from the shifts of signals using a multiexponential fit with convolution. The ${}^M\sigma_i$ are also obtained from the fit procedure.

Special features of transient dissociative ionization and the method of assignment are discussed in ref 9. In the two dialkyl derivatives that are investigated in this work, the similarities were such that assignment and evaluation were entirely analo-

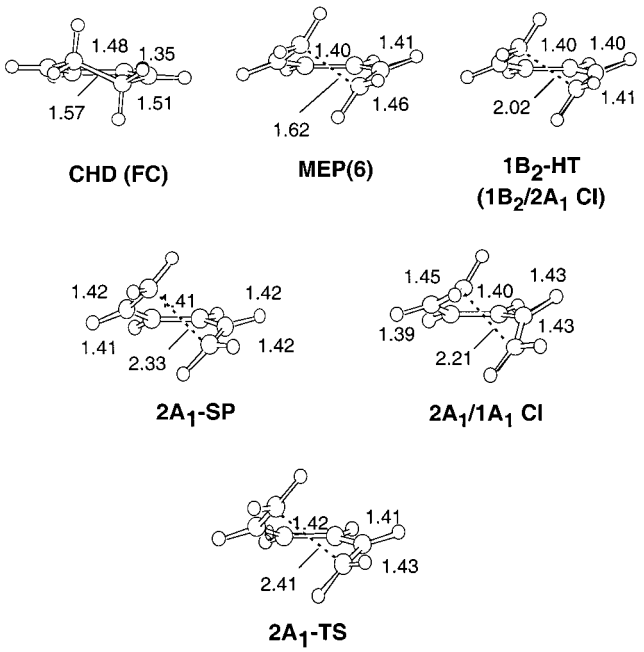

Figure 2. Relevant molecular structures along the $1B_2 \rightarrow 2A_1$ pathway of CHD. The geometrical parameters are given in Å. The structures have been computed at the CASSCF level of theory.

gous. Chemicals (Fluka) were used after degassing without further purification. According to gas-chromatography mass-spectrometry they contained 1−3% of impurities; these did not disturb the measurements, however, since they either absorb at shorter wavelengths than the pump radiation (1,4-cyclohexadiene) or else contribute only a time-independent signal (benzene and substituted benzenes, i.e., the dehydrogenation products). The products of ring opening were present in concentrations of less than 0.2%.

3. Results

3.1. Computational Results. The complete excited-state MEP for CHD has been presented in previous work.[4−6] There are five key structures which describe the evolution of the photoexcited reactant and its decay to the ground state. These correspond to the structures CHD (or FC), MEP(6) and $1B_2$−HT (i.e., the $1B_2/2A_1$ CI) located on the $1B_2$ energy surface and the $2A_1$−SP and $2A_1/1A_1$ CI located on the $2A_1$ energy surface. These structures are compiled in Figure 2 and their positions and order along the reaction path are indicated in Figure 1.

The initial relaxation of CHD out of the spectroscopic state $1B_2$ does not occur in a straightforward way along a single coordinate; rather, it takes place in two distinct steps.[6] Comparison of the CHD (FC in Figure 1) and MEP(6) structures shows that initially the bond lengths and twist angles in the π system change rapidly, but become constant after point MEP(6). After MEP(6), the ring opens and the C_5-C_6 distance reaches about 2.0 Å at $1B_2$−HT (the lowest energy point we could locate on the $1B_2$ state). The molecule is then released to the $2A_1$ state in the region of a $1B_2/2A_1$ CI located near $1B_2$−HT. Note that at this point *the stereochemical decision regarding the conrotatory or disrotatory direction of ring opening has already been taken*. In fact, the two CH_2 twist angles have become large and of equal sign for the two groups, corresponding to a conrotatory deformation.

To elucidate the motion associated with this decay, we have computed the branching space defined by the GD and NADC vectors (see section A.1). These vectors are shown in Figure 3.

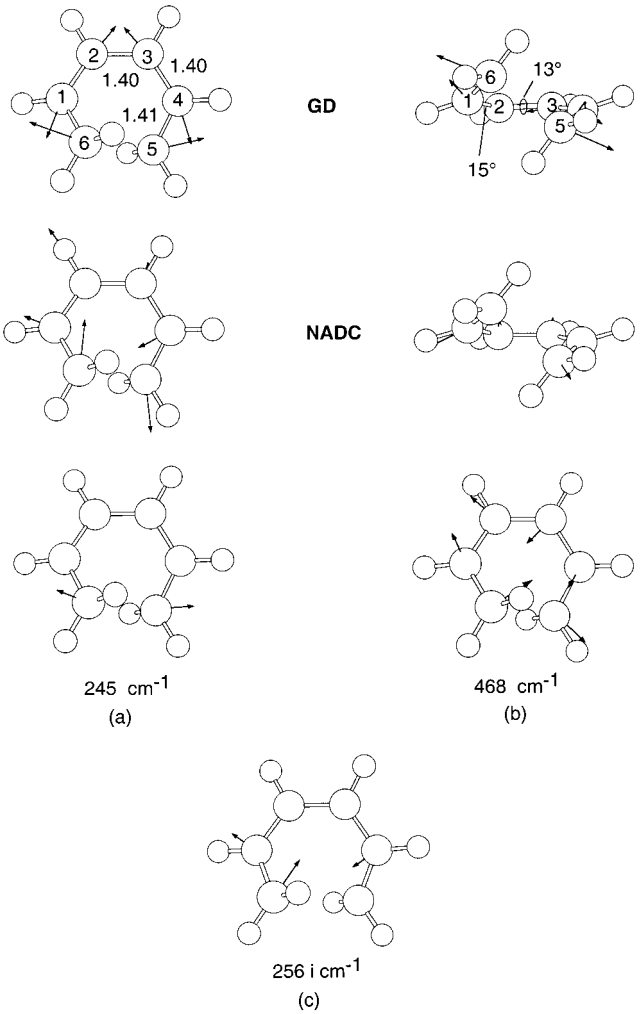

Figure 3. (a) Gradient difference (GD) and nonadiabatic coupling (NADC) vectors for the structure $1B_2$−HT ($1B_2/2A_1$ CI). The geometrical parameters are given in Å and degrees. (b) $1B_2$ vibrational modes at the same point. (c) Transition vector at $2A_1$-TS. For simplicity the carbon atoms are numbered according to the corresponding CHD structure.

The GD vector roughly coincides with the reaction coordinate and describes the ring opening process accompanied by double-bond single-bond interchange. In contrast, the NADC vector corresponds to a completely antisymmetric mode, describing, roughly, an out-of-phase combination of the bending of the $C_2-C_1-C_6$ and $C_3-C_4-C_5$ angles. The shape of the $1B_2$ and $2A_1$ energy surfaces along the branching space is given in Figure 4a. Single point MS−CASPT2 calculations on a 5×5 grid of points within the branching space, demonstrate that the two energy surfaces do indeed intersect along a coordinate parallel to the GD vector. At the $1B_2/2A_1$ CI, the surface crossing is allowed by the different symmetry of the $1B_2$ and $2A_1$ wave functions. Along the symmetry-breaking NADC direction, the $1B_2/2A_1$ degeneracy is gradually lifted. This surface indicates that after progression along the C_2-symmetric relaxation path on the $1B_2$ sheet the molecule must undergo a symmetry-breaking displacement in order to decay to the $2A_1$ state. In other words, the totally symmetric reaction path along the $1B_2$ energy surface must rapidly turn into a fully asymmetric direction, such that the conical intersection is "avoided" and the associated S_1 wave function changes from that of the $1B_2$ to that of a $2A_1$ state. This behavior is pictorially illustrated in Figure 4b.

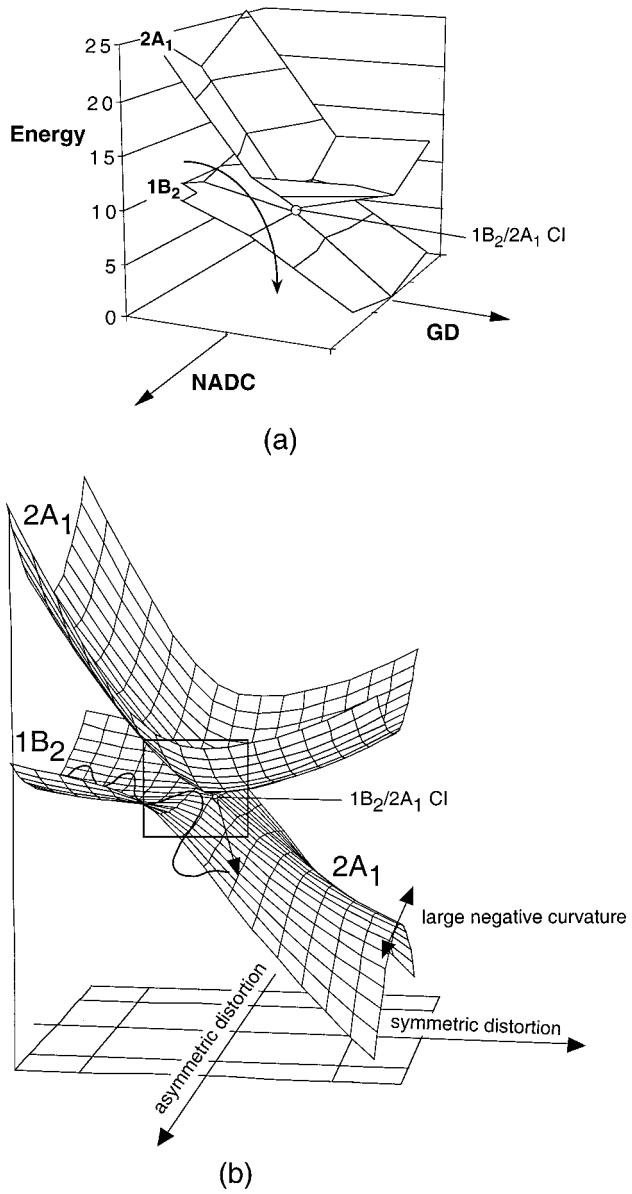

Figure 4. (a) MS−CASPT2 computed $1B_2/2A_1$ conical intersection region along the GD and NADC vectors. Only a 3×3 portion of the 5×5 computed grid is shown for clarity. The curved arrow illustrates the direction of the reaction coordinate in this region. Because of the conical intersection, symmetry breaking deformation has already begun on the $1B_2$ energy surface. (b) Pictorial illustration of the potential energy surface structure in the vicinity of the $1B_2/2A_1$ conical intersection. The frame indicates the position of the energy surfaces given in part a. The picture shows that negative curvature increases toward the CI.

Further evidence for the potential energy structure given in Figure 4b comes from frequency computations in the vicinity of the conical intersection. IRD computations at the $1B_2/2A_1$ CI[5] show that the driving force for the initial relaxation along the $2A_1$ surface has its largest component along the NADC direction. Frequency computations[5] show that, in the vicinity of the $1B_2/2A_1$ CI point, the $2A_1$ surface features a large negative curvature (in imaginary wavenumber units, up to 2700i cm^{-1}) along an asymmetric mode similar to the NADC vector. This implies that the shape of the $2A_1$ energy surface is a ridge along a C_2 symmetric cross section. Furthermore, a frequency computation on the $1B_2$ state demonstrates that the corresponding surface is stable with respect to the same kind of molecular deformations featuring a symmetric and an antisymmetric mode with wavenumbers 245 and 468 cm^{-1}, respectively (modes (a) and (b) in Figure 3). A positive curvature on the upper sheet and a negative one on the lower sheet is typical of the surrounding regions of conically intersecting surfaces. Thus, we now have the explanation of the large negative curvature found in ref 5.

The structure of the low lying region of the $2A_1$ potential energy surface is given in Figure 5. It can be seen that the $2A_1-$SP and $2A_1/1A_1$ CI structures are located on an extremely flat region of the $2A_1$ energy surface.[5] This region, which lies about 10 kcal mol^{-1} below the $1B_2/2A_1$ CI, is spanned by a complex bending deformation which connects the two pairs of asymmetric structures $2A_1-$SP and $2A_1/1A_1$ CI with each other via the C_2-symmetric structure $2A_1-$TS. It is remarkable that the NADC vector of the $1B_2/2A_1$ CI is similar to the transition vector at $2A_1$-TS (mode (c) in Figure 3) which points to the $2A_1$ minimum ($2A_1-$SP) and continues towards the $2A_1/1A_1$ CI (see structures in Figure 2). This indicates that the flat $2A_1$ valley is oriented in a direction roughly parallel to the NADC vector of the $1B_2/2A_1$ CI.

The surface shape suggests that the wave packet is accelerated, upon exit from the $1B_2/2A_1$ CI, toward the asymmetric $2A_1-$SP and $2A_1/1A_1$ CI. Such a motion is illustrated by the trajectories depicted in Figures 4b and 5. However, before hitting the $2A_1/1A_1$ CI, the wave packet will, in general, need several oscillations in the region of the $2A_1-$SP energy minimum, and this vibration on the shallow plateau will have a low frequency. This expectation is not in line with the observed time of 77 fs for $2A_1$ decay. To find an explanation for this behavior, we investigate the hypothesis that other $2A_1/1A_1$ conical intersections exist on the $2A_1$ energy surface, that are more readily accessible than the previously reported $2A_1/1A_1$ CI. There are two limiting cases: (a) a conical intersection is entered immediately after $1B_2 \rightarrow 2A_1$ decay as an effect of the initial acceleration along the $1B_2$ energy surface. In particular, the momentum acquired on the $1B_2$ energy surface and pointing along the GD vector may be sufficient to displace a part of the wave packet toward a conical intersection lying closer to the C_2-symmetric crossing, thus inducing a faster decay, (b) an extended set of easily accessible conical intersection points exist on the low lying part of the $2A_1$ energy surface so that one of these points is intercepted within a few oscillations during the motion following $1B_2 \rightarrow 2A_1$ decay.

To explore the hypothesis (a), we have computed the lowest lying $2A_1/1A_1$ conical intersection point with C_2 symmetry (C_2-CI, maximum of the solid line in Figure 5). The molecular structure of this CI is given in Figure 6, where we also show the corresponding GD and NADC vectors. These vectors are both (and for symmetry reasons must be) totally symmetric. It is therefore obvious that the branching space of the symmetric $2A_1/1A_1$ CI is fundamentally different from that of the symmetric $1B_2/2A_1$ CI; for the latter, the NADC vector must be antisymmetric.

The GD and NADC vectors of C_2-CI (Figure 6) can also be compared with those of the lowest lying (asymmetric) conical intersection $2A_1/1A_1$ CI (Figure 7). The branching space of these two decay channels appears to be unrelated. In fact, the C_2-CI GD and NADC vectors of Figure 6 are dominated by symmetric expansion of the two terminal C−C bonds and two middle C−C bonds, respectively. In contrast, the branching space vectors of Figure 7 are dominated by bending modes.

To reach the C_2-CI, the system would have to undergo a large displacement with an increase in the torsional angles $C_6-C_1-C_2-C_3$ and $C_2-C_3-C_4-C_5$ from 14° to 37°, together with

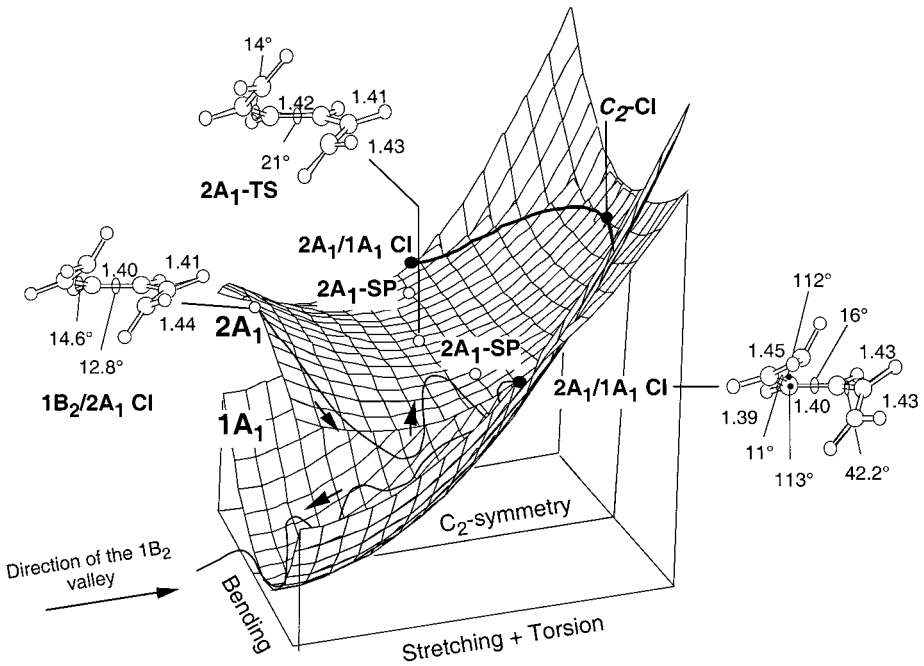

Figure 5. Pictorial illustration of the structure of the low-lying part of the $2A_1$ potential energy surface. The solid line indicates the minimum energy path connecting the symmetric (C_2−CI) and asymmetric ($2A_1/1A_1$ CI) conical intersections and lying within the $2A_1/1A1$ intersection space. The labels refer to structures of Figure 2. The geometrical parameters are given in angstroms and degrees.

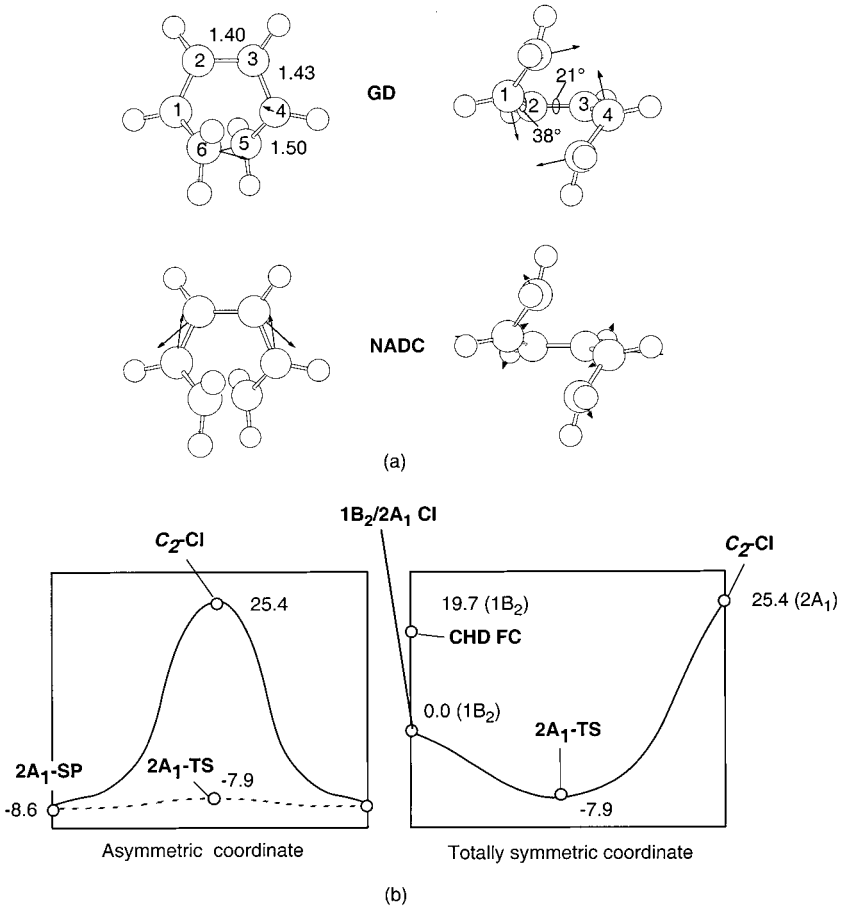

Figure 6. (a) Structure with gradient difference (GD) and nonadiabatic coupling (NADC) vectors for the symmetric $2A_1/1A_1$ conical intersection (C_2−CI). The geometrical parameters are given in angstroms and degrees. The carbon atoms are numbered according to the corresponding CHD structure. (b) Energy profiles of the $2A_1$ potential energy surface along the asymmetric (left) molecular distortions $2A_1$−SP→C_2−CI (solid line) and $2A_1$−SP→$2A_1$−TS (dashed line) and totally symmetric (right) molecular distortion $1B_2/2A_1$ CI→C_2−CI. The relative energy values are from Table 1.

expansion of the C_1−C_6 and C_4−C_5 bonds (compare the structures in Figure 3 and Figure 6). However, this point is located 5.7 kcal mol^{-1} above the CHD FC point (see Figure 6). To reach this point, the molecule would have to conserve a

TABLE 1: Absolute and Relative Energies Computed at the CASSCF and MS−CASPT2 Level of Theory

structure[a]	state[c]	CASSCF energy/au	MS−CASPT2[d,e] energy/au	relative MS−CASPT2 energy/kcal mol^{-1}
1B−HT ($1B_2/2A_1$ CI)[b]	$1B_2$	−231.66999	−232.46946	0
	$2A_1$	−231.71271	−232.46203	4.7
	$1A_1$	−231.80391	−232.53646	−42.0
$2A_1$−SP	$2A_1$	−231.73632	−232.48314	−8.6
	$1A_1$	−231.79374	−232.51978	−31.6
$2A_1/1A_1$ CI	$2A_1$	−231.72424	−232.46426	3.3
	$1A_1$	−231.72429	−232.48066	−7.0
C_2−CI	$2A_1$	231.69683	−232.42897	25.4
	$1A_1$	−231.69694	−232.43752	20.4
$2A_1$−TS	$2A_1$	−231.73700	−232.48211	−7.9
	$1A_1$	−231.80090	−232.52439	−34.5
FC	$1B_2$	−231.61112	−232.43809	19.7
	$2A_1$	−231.64242	−232.39588	46.2
	$1A_1$	−231.88084	−232.62694	−98.8

[a] All molecular structures are fully optimized at the CASSCF level of theory with the 6-31G* basis set. [b] The 1B−HT does not show a conical intersection at the CASSCF level because dynamical correlation is essential to describe the $1B_2$ and $2A_1$ energies in a balanced way. [c] For the asymmetric $2A_1/1A_1$ CI structure, the symmetry labels indicate the character which dominates the corresponding wave function. [d] Multistate mixing is (predictably) not observed in the symmetric points $2A_1$−SP, $2A_1$−TS (these points are far from degenerate) and $1B_2/2A_1$ CI (this is a conical intersection between two states of different spatial symmetry). It is significant in $2A_1/1A_1$ CI and C_2−CI (these are conical intersection points between states of the same spatial symmetry). In these cases, the effect of the multistate correction is to split the energies slightly. This splitting is assumed to be due to a difference between the CASSCF optimized geometry used in this work and the MS−CASPT2 optimized geometry. This last geometry is at present computationally intractable. [e] In all cases no intruder states were found with a weight of the zeroth-order wave function >0.75.

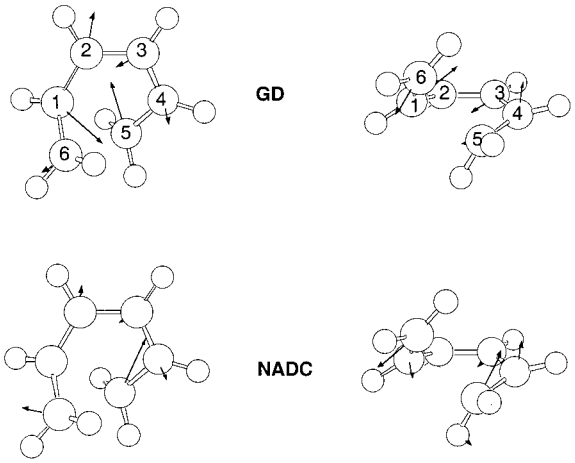

Figure 7. Gradient difference (GD) and nonadiabatic coupling (NADC) vectors for the asymmetric $2A_1/1A_1$ conical intersection ($2A_1/1A_1$ CI). The carbon atoms are numbered according to the corresponding CHD structure.

large excess energy along the totally symmetric mode, and this is highly unlikely. As shown in Table 1, C_2−CI intersection is 22 kcal mol^{-1} higher in energy than the asymmetric intersection $2A_1/1A_1$ CI.

Despite the very different molecular structure, energy and branching space, the C_2−CI and $2A_1/1A_1$ CI structures are conical intersections between the same two potential energy surfaces and, in principle, mediate the same photochemical ring-opening process. Therefore, a fundamental question to be answered is whether these two points are elements of the *same* intersection space. In this case, there will be a *continuous line* of conical intersection points (i.e., a line residing in the (f − 2)-dimensional intersection space) connecting the symmetric and asymmetric CI points. Thus, to find such a connection and explore hypothesis (b), we apply the new method mentioned in section 2.1 (see also section A.1) to map out the steepest descent line from C_2−CI within the intersection space. The resulting line is given in Figure 8 and is also schematically reported in Figure 5.

The CASSCF results (Figure 8a) demonstrate, to within the numerical error, that there indeed exists a line of conical intersection points connecting the two CIs. Along this line, both the geometrical structure and the directions of the GD and NADC vectors smoothly change from those of Figure 6a to those of Figure 7. The possible role of this space in increasing the rate of decay from the $2A_1$ surface of CHD will be discussed below. Note that the reevaluation of the $2A_1$ and $1A_1$ energy profiles along the same computed path using the higher level CASPT2 and MS−CASPT2 methods (see Figure 8b) decrease the level of degeneracy of the two profiles (more evident for the MS−CASPT2 result). However the profiles remain roughly parallel and with a modest energy gap. The degeneracy is most probably decreased because of the change in the actual position of the MEP (i.e., the change in the MEP coordinate) when passing from the CASSCF to the CASPT2 and MS−CASPT2 energy surfaces. MEP calculations as well as geometry optimizations at the CASPT2 and MS−CASPT2 levels are presently not feasible.

3.2. Experimental Results. Figure 9 shows the gas-phase UV spectra of CHD and its 1,4- and 2,5-methyl-isopropyl derivatives (α-terpinene and α-phellandrene, respectively). The spectrum of CHD agrees with earlier measurements, except for a small shift in the condensed phase (gas,[17,18] solution,[17] or matrix[19]). For the derivatives, only poorly resolved solution spectra have been previously reported.[20] The broad longest wavelength band corresponds to the transition to the $1B_2$ state. Only terpinene shows a clearly visible vibrational structure in this band (spacing 1350 cm^{-1}, marked by vertical bars). In contrast, the spectra of CHD and phellandrene are completely continuous with only traces of vibrational structure. For CHD, the structure was enhanced by electronic filtering (as in ref 21, not shown); the position of the peaks thus found are marked by vertical arrows (spacing 1450 cm^{-1}).

A recent high-level ab initio calculation (CASPT2) for 1,3-cyclohexadiene places the transition to the $2A_1$ state (which at this geometry has Rydberg 3s character) at 5.49 eV (226 nm), in the short-wavelength wing of the $\pi\pi^*$ transition to $1B_2$.[22] In the same work, this state has been localized by (2 + 1)-REMPI spectroscopy at 5.39 eV. But conventional spectroscopy (with

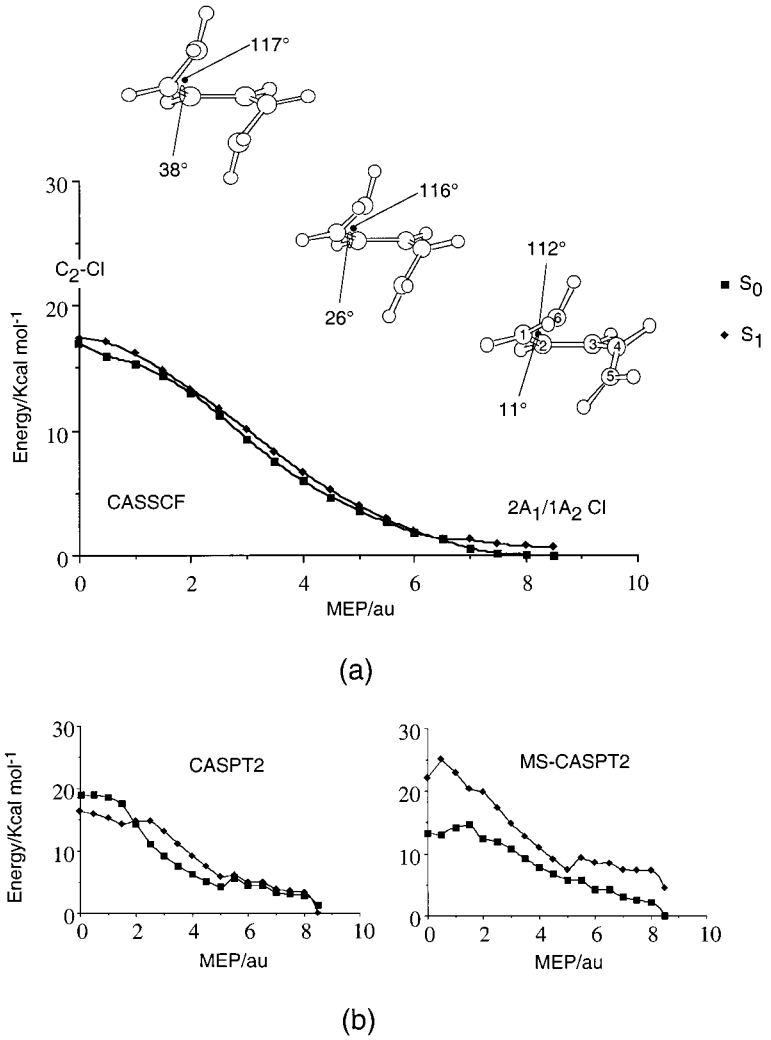

Figure 8. (a) MEP from C_2-CI to $2A_1/1A_1$ CI within the $2A_1/1A_1$ intersection space. The structures illustrate the progression from C_2-CI to $2A_1/1A_1$ CI (the dominant $C_6-C_1-C_2-C_3$ dihedral and $C_6-C_1-C_2$ planar angles are given in degrees). The carbon atoms are numbered according to the corresponding CHD structure. (b) Energies recomputed at the CASPT2 and MS−CASPT2 levels of theory. The MEP coordinate is in mass-weighted Cartesians (au = $u^{1/2}$ a_0).

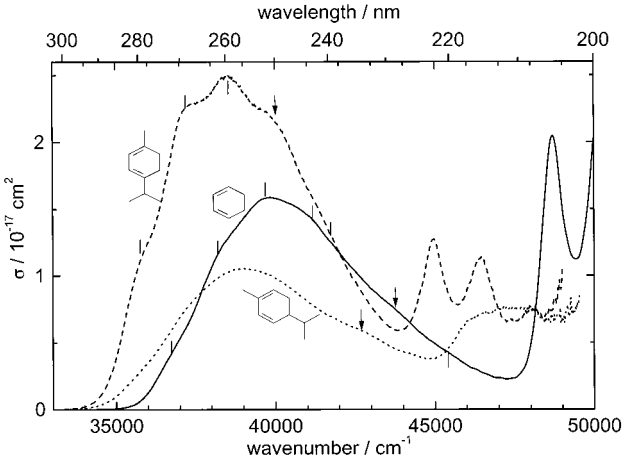

Figure 9. Gas-phase UV spectra of CHD (full line), α-terpinene (dashed line) and α-phellandrene (dotted line). Vibrational structure is marked by vertical bars. The arrows indicate the $2A_1$ bands.

electronic filtering) also reveals it: The spectrum shows a peak or shoulder at 228.5 nm (5.43 eV, marked by an arrow, with a vibrational satellite at 1690 cm^{-1} higher energy) which does not join the longer-wavelength vibrational progression. Further evidence for the $2A_1$ assignment comes from the derivatives: the substituents in terpinene lower the ionization energy of CHD (8.25 eV[23]) by 0.58 eV;[24] Rydberg terms should be lowered by a similar amount. In fact, the peak at 252 nm exactly corresponds to the calculated position (with the peak at 222.5 nm also in reasonable agreement with a calculated Rydberg 3p term[22]). Similarly, from the reported ionization energy of 8.01 eV of phellandrene,[24] the $2A_1$ band is predicted at 234 nm, in good agreement with the peak observed at 236 nm. So in each compound the peak marked by the arrow can be assigned to the $1A_1 \rightarrow 2A_1$ transition.

From the *time-dependent signals* of several ions, we determined time constants (lifetimes including transit times) τ_i for the observation windows *i* indicated in Figure 1. The procedure was the same as before:[9] Time constants $\tau_i \geq 40$ fs were determined from exponential tails of suitable ion signals at delay times larger than the pulse lengths, equivalent to a multiple of τ_i. Shorter times (i.e., only τ_1 of CHD and phellandrene) are from full simulation of the signals (section 2.2), in particular of the rising part and maximum. It may be surprising that we can report several τ_i below the pulse lengths, but this is because they are recovered from several independent signals. This aspect is discussed in ref 16. The τ_i thus found are listed in Table 2 for cyclohexene (published previously[9]) and the two derivatives. The table also indicates the relative probabilities ${}^M\sigma_i$ to produce

TABLE 2: Experimental Results and Simulation Parameters for the Six-level Rate-Equation Model[a]

window (i)	1	2	3	4	5	6
1,3-Cyclohexadiene						
τ_i/fs[b]	10 ± 5	43 ± 3	77 ± 7	≥ 35[c]	≤ 20[c]	$>5 \times 10^4$
$^{80}\tau_i$	1.0	0.23	0	0	0	0
$^{79}\tau_i$	1.0	0.87	0.53	0	0	0
$^{39}\tau_i$	1.0	0	0	0.7	0.7	0.05
$^{27}\tau_i$	1.0	0	0	0.9	0.9	0.096
$^{1}\tau_i$	0	0	0	0	1.0	0.068
τ_{prod}/fs			205			
τ_{rot}/fs[b]			580 ± 75			
α-Terpinene (1-Methyl-4-isopropyl-1,3-cyclohexadiene)						
τ_i/fs[b]	40 ± 5	59 ± 4	86 ± 6	≥ 35[c]	≤ 20[c]	$>5 \times 10^4$
$^{136}\tau_i$	0.36	1.0	0	0	0	0
$^{121}\tau_i$	0	1.0	0.42	0	0	0
$^{1}\tau_i$	0	0.317	0	0	1.0	0.05
τ_{prod}/fs			270			
τ_{rot}/fs[b]			630 ± 125			
α-Phellandrene (2-Methyl-5-isopropyl-1,3-cyclohexadiene)						
τ_i/fs[b]	10 ± 5	66 ± 4	97 ± 6	3[c]	3[c]	$> 5 \times 10^4$
$^{136}\tau_i$	1.0	0.28	0	0	0	0
$^{93}\tau_i$	1.0	0.75	0.17	0	0	0
$^{1}\tau_i$	0	0	0	1.0	1.0	0.016
τ_{prod}/fs			205			
τ_{rot}/fs[b]			720 ± 150			

[a] τ_i is the lifetime of level i (traveling time through observation window i) and $^M\sigma_i$ the relative ionization cross-section (normalized to a maximum of 1.0 in each line) to produce an ion of mass M from the ith level. τ_{Prod} is the time needed to form 63% of the product in its ground state (the ring-opening time calculated from $\tau_1-\tau_5$), τ_{Rot} the time of rotation, derived from rotational anisotropy decay of the H^+ signal. The assignment of the time constants τ_i to different locations (windows) on the potential energy surface is given in Figure 1. Window 6 represents the end product and τ_6 its minimum lifetime. [b] All values averaged over at least ten independent scans. Error limits for $\tau_i \geq 40$ fs represent standard deviations in this averaging, and for the two shorter times ($\tau_1 = 10$ fs) they are estimated limits within which a reasonable fit can be obtained. [c] $\tau_4 + \tau_5 = 55 \pm 6$, 55 ± 6 and 6 ± 3 fs for the three compounds, respectively. In phellandrene, one level preceding the final one on the ground-state surface would be sufficient to simulate the signals. But by analogy to CHD and terpinene we assumed two, levels 4 and 5, with equal lifetimes (τ_4 and τ_5).

an ion of mass M from window i; the superscript M indicates at the same time which ions were used for evaluation. It can be seen that the parent ion is only found at the earliest stages, whereas the smallest fragments (down to H^+) are produced from the product ground state. Bearing in mind that vibrational energy is released as the neutral molecule describes a path down the potential energy surface, this observation was interpreted by assuming that much of this energy is taken over to the ion, causing fragmentation within it.[9,25] Note that the neutral species does not photochemically break down in the short observation time, whereas the ion has sufficient time (tens of nanoseconds) for fragmentation before acceleration and detection in the mass spectrometer.

Previous time-resolved work on phellandrene reported a ring-opening time (τ_{prod}) of 11 ps.[26,27] But it did not have adequate time resolution (see the discussion in ref 9). Most time constants are similar for the three compounds. A conspicuous difference is the fourfold times longer τ_1 in terpinene which will be discussed in sections 4 and 5. For phellandrene, simulation of all signals was also perfectly satisfactory with a single window (transit time 6 ± 3 fs) preceding the final one on the ground-state surface; however, for consistency we chose two and distributed this short time equally to τ_4 and τ_5. (Window 4 was assigned to a region of an accidental resonance with the probe laser.[9] Such a resonance seems also to be present in terpinene, but not in phellandrene.)

Table 2 also gives two additional ground-state constants (τ_{rot} and τ_{prod}) for each compound. The time of rotation τ_{rot} (implying the moment of inertia) was determined from the decay of anisotropy in the same way as in ref 9; since it was derived from a late-time signal (400−1000 fs), it belongs to the product, and the size indicates that it is the *cZc*-hexatriene (or derivative). This product forms in a multistep process, so that a single-exponential function cannot give a good fit. Nevertheless, to give a number for orientation, we define τ_{prod} as the time after which 63% ($= 1 - e^{-1}$) has formed and *calculate* it from the rate equations with the experimental $\tau_1-\tau_5$. The present work focuses on the excited-state processes ($\tau_1-\tau_3$). The following ground-state processes are analogous to those discussed for CHD in ref 9.

4. Discussion

The new results on the structure of the region surrounding the $1B_2/2A_1$ CI and on the line of conical intersections connecting the $2A_1/1A_1$ CI with the C_2−CI shed new light on the mechanism of photoinduced electrocyclic ring openings. To rationalize the short τ_3, it has been suggested[8] that the S_1 molecule is *directly* accelerated toward a conical intersection (CI). However, the computed minimum energy path does not lead to the $2A_1/1A_1$ CI, but to a $2A_1$ minimum where, if momentum effects are neglected, the system may lie for several hundred femtoseconds before decaying through the nearby lowest lying CI. Such a long time is also implied by the activation entropy calculated in ref 4. In this case, the mechanistic picture of Phase 3 would be similar to the one already discussed for the *trans*−*cis* isomerization of polyenes, such as *all-trans*-hexa-1,3,5-triene, where relaxation to an excited-state energy minimum precedes evolution towards a conical intersection funnel.[5] Indeed, a time of about 450 fs was found for departure from the S_1 state of this molecule[28,29] and of 5000 to 750 fs for *cis*-hexa-1,3,5-triene depending on excess energy.[21]

It is worth noting that the problem is not much mitigated by replacing the trajectories with wave packets; they have a certain extension in the coordinate space so that they can overlap with a CI point even without directly hitting it. A recent study of the quantum dynamics on the cyclohexadiene $2A_1$ surface found that such a near encounter can already occur within ≤ 30 fs following release from the first conical intersection (depending to some extent on the initial conditions).[30] However, only a small part of the wave packet in the immediate surrounding of the CI will decay through the funnel; the largest part was estimated to oscillate on the $2A_1$ plateau for ≥ 200 fs before finding the exit through the $2A_1/1A_1$ CI.[30]

We attribute the time < 100 fs observed for Phase 3 to the combined effects of the energy surface shape about the $1B_2/2A_1$ CI and the accessibility of the low-lying $2A_1/1A_1$ intersection space for decay to the ground state. In fact, in section 3.1 we found that the system must go *around* the lower cone of $1B_2/2A_1$ CI thus being displaced in the direction of the asymmetric NADC vector. Hence the molecule is accelerated, by virtue of the negative curvature of the $2A_1$ surface, toward the flat plateau containing the $2A_1$ energy minimum $2A_1$−SP and the $2A_1/1A_1$ CI. (By contrast, in *all-trans*-hexatriene, such a curvature is negligible and the molecule relaxes along a totally symmetric path down to a symmetric $2A_1$ minimum.[5]) While the relaxation direction does not directly lead to the optimized $2A_1/1A_1$ CI (Figure 5), the decay to the ground state is greatly

facilitated by the fact that this environment contains the $(f-2)$-dimensional intersection space. Thus, the lowest lying part of this space is represented by the minimum energy path from the C_2−CI to the $2A_1/1A_1$ CI (Figure 5 solid line, and Figure 8a). The direct acceleration to an outlet of the funnel not only explains the short τ_3, but also the observation that the wave packet is still very compact after passing the last conical intersection (concluded from the narrow H^+ signal in ref 9). In fact, diffusing around on the flat $2A_1$ plateau would certainly broaden the wave packet.

In the three-phase picture of the excited-state reaction coordinate, it is striking that the 1,4-substituted derivative terpinene needs four times longer to leave the FC region (Phase 1) than cyclohexadiene itself. The more pronounced vibrational structure in the UV spectrum of terpinene (Figure 9) probably reflects this longer lifetime. A natural explanation is a mass effect of the 1,4-substituents: in Phase 1 the FC structure (equilibrium geometry of CHD) evolves to structure MEP(6) (see Figure 2). These two structures not only differ in the bond lengths of the π system, but also in an out-of-plane twisting of the two substituents in positions 1 and 4. Increasing the mass of the substituents (replacing two hydrogen atoms in CHD) will clearly slow this motion. The fact that, in the other windows, time lengthening is only minor shows that different groups are involved in the associated motions.

Similarly the fact that the 2,5-substituted derivative phellandrene exhibits no time lengthening in Phase 1, shows that the 2,5-groups are not strongly involved, just as predicted by the calculations. However, phellandrene seems to spend 1.5 times longer than CHD in Phase 2 where the motion is definitely dominated by the breaking of the σ bond between C_5 and C_6. This lengthening can be rationalized by comparing the structures MEP(6) and $1B_2/2A_1$ CI, in which the two halves of the CHD framework come apart from each other, moving the mass of the substituent in position 5. A certain conrotatory twist of the 1,4-substituents is also involved, so it is understandable that τ_2 also increases to some extent in terpinene (by ca. 35%, compared with CHD). The variations in τ_3 are even smaller, in agreement with the path calculated for this phase which is dominated by asymmetric bending of the backbone.

It may be asked why we did not consider energetic effects of the substituents. In fact, it has been reported that alkyl groups on the π system lower the $1B_2$ state, whereas the $2A_1$ state is practically unaffected.[31] However, the computed surface topology of Figure 4 indicates that the energy and structure of the $1B_2/2A_1$ CI should only slightly change upon stabilization of the $1B_2$ state relative to the $2A_1$ state. In particular, lowering the $1B_2$ energy surface, which is very flat in this region, will just shift the intersection to a slightly larger $C_1\cdots C_5$ distance. While these changes may contribute to the observed slight increase of Phase 2 lifetime for the substituted system (see Table 2), the structures of the relaxation pathways are expected to remain essentially unchanged.

5. Interpretation in Terms of Driving Forces

In this section, we try to interpret the excited-state motion of the molecule in terms of the variation in the direction of energy slopes. Since slopes of potential energy surfaces are forces, we can talk of the "driving forces" of the photoreaction.

5.1. The Processes on the Spectroscopic Surface: Where Are the Woodward−Hoffmann Rules Switched on? In sections 3 and 4, the first time constant was assigned to the departure from the FC region. By definition, FC active coordinates are those along which the excited state minimum is shifted (totally symmetric coordinates). This gives rise to a nonzero slope in the FC region. Since the excitation is of $\pi\pi^*$ type, we can expect that it is primarily the π system that is involved, showing in particular CC stretching, but also (though with flatter initial slope) double-bond twisting. This is exactly what the calculation shows: In Figure 2 these lengths and angles change rapidly from the beginning, whereas others become substantially involved only after point MEP(6) (see also Figure 1 in ref 6). It follows that the initial acceleration is along a combination of FC active coordinates, a statement that has a general validity extending beyond pericyclic reactions. For instance, in the *cis*−*trans* isomerization of retinal chromophores, a CC stretch precedes the actual isomerization.[5,32] In CHD this early distortion showed up in the resonance Raman data which detected a conrotatory twist of the two CH_2 groups already in the Franck-Condon region.[33]

Backbone distortion of cyclohexadiene also twists the C_5-C_6 σ bond in such a way that it becomes more parallel to the p orbitals of the π system, thus facilitating the $\sigma\pi$ interactions which are required by the WH interaction. The motion along the FC active coordinates can, therefore, be considered to be a preparation to activate the WH rules. Also this statement seems rather general: in all photochemical pericyclic reactions, it is the π system which is excited, but σ bonds are always involved in the reaction, and very often the σ bonds initially have an unfavorable orientation for interaction with the π system.

In the case of cycloheptatriene, it has recently been shown that the molecule initially moves along FC active coordinates and only later turns to the predicted WH mode. Indeed, the deuterium isotope effect on the time constants showed that the hydrogen only begins to move in the second observation window, but still on the spectroscopic surface.[34] Note that the present work reports similar evidence for cyclohexadienes.

5.2. Symmetry Breaking, and the Motion on the S_1 Surface and through the Conical Intersections. The traditional way of deriving the WH rules is to assume that one symmetry element is conserved during the reaction. This symmetry conserving coordinate has been used to derive the original van der Lugt−Oosterhoff diagram (Figure 1). The result reported above yields a refinement of this picture by showing that the molecule evades a symmetric coordinate already on the $1B_2$ surface. This arises because the wave packet enters (along the initial symmetric coordinate of the branching space) on the lower cone of the CI which itself has C_2 symmetry. The cone generates a deflection along the NADC vector (see Figure 4). Symmetry breaking is hence caused by the existence of a cone-shaped energy surface along the symmetry conserving path. More generally, it is clear that a minimum energy path (i.e., the reaction coordinate) developing along the *lower* energy surface of a conical intersection will *avoid* the crossing point which corresponds, locally, to an energy maximum (actually to the lower cone apex). In contrast, a minimum energy path developing along the *upper* energy surface of the conical intersection *will be attracted to* the crossing point which corresponds to a local "funnel".

5.3. The Principle of Least Motion as a Consequence of Slopes. Throughout this work, we have considered the slopes of the potential energy surfaces. Since slopes are forces this concept appears to be intuitive for a chemist. To illustrate its potential, we give here a new rationalization of the principle of least motion, which has been formulated in the context of ring opening of phellandrene[35] (see also the review[36] on the photochemistry of small polyenes). We should first note that phellandrene is a mixture of two conformers with comparable

abundance at room temperature.[35] (The fact that we observed only one set of time constants implies that the rates of the two different conformers are rather close to each other). They have the 5-isopropyl group in the equatorial and axial positions, respectively. Each conformer yields just one product on ring opening: the equatorial form gives a hexatriene with the isopropyl group in the *E* position at the double bond, whereas the axial one yields the *Z* isomer. The WH rules would allow both products from each conformer, depending on whether the conrotatory motion occurs clockwise or counterclockwise. However, the principle of least motion and its special case, the accordance principle, state that one of these directions will be negligible, in favor of the pathway involving least displacement of the atoms and groups taking part.[35] Our interpretation invokes a guiding by the slopes: Whereas on the upper surface there are probably steep slopes in both clockwise and counterclockwise directions, vertical excitation of a pre-twisted molecule (i.e., the half-chair conformation of CHD) will arrive at only one of them, and the rapid acceleration precludes the sampling of other directions. This is an example where the stereochemical decision is already taken in the Franck−Condon region. Previous explanations have tried to invoke electronic effects, based on orbital interactions claimed to be different for the different rotations.[35]

6. Conclusion

With the detailed reaction path calculated on the excited surfaces and the five time constants (three of them for the excited states) reported in Figure 1 and Table 2, the ring opening of cyclohexadiene is now one of the experimentally and theoretically best documented photochemical reactions. (Previous time-resolved experiments only determined how fast the initial excited-state disappears or the product appears.[37]) It should first be noted that all windows are passed in times less than 100 fs. This is near the *maximum conceivable speed*, as can be seen by comparison with the period of an appropriate vibration. For instance, τ_3 (77 fs in the unsubstituted cyclohexadiene), the time for leaving the S_1 state, is only a fraction of the period of a vibration on the very flat $2A_1$ plateau; a period of 77 fs would correspond to a wavenumber of 433 cm^{-1}.

We have shown that the momentum accumulated along a C_2-symmetry conserving direction is not sufficient to reach the symmetric C_2−CI point of the intersection space, since it is higher in energy than the Franck−Condon region. However, the calculations demonstrated the existence of a line of CIs connecting the C_2−CI with the minimum energy CI (the $2A_1/1A_1$ CI). The wave packet (with some momentum) can easily hit the continuum of CI points located on the lower part of this line and can thus immediately cross over to the ground state. This mechanism explains the "maximum speed" observed for the departure from the $2A_1$ surface. The cyclohexadiene case seems to be typical of many pericyclic reactions, a statement suggested by the similarly short times found in a number of such reactions.[38] A simple diagram consistent with the present knowledge of the ring opening coordinate is given in Scheme 1. This diagram represents a refinement of the original van der Lugt−Oosterhoff diagram of Figure 1.

It should be noted that, in the new diagram, a $1B_2/2A_1$ avoided crossing replaces the $1B_2/2A_1$ real crossing of the original diagram. Similarly a $2A_1/1A_1$ conical intersection hyperline replaces the $2A_1/1A_1$ single point. This difference is highlighted in Scheme 1 by including in the reaction coordinate the representation of the asymmetric $2A_1/1A_1$ conical intersection structure (see Figures 5 and 7). In Scheme 1, we also assume

SCHEME 1

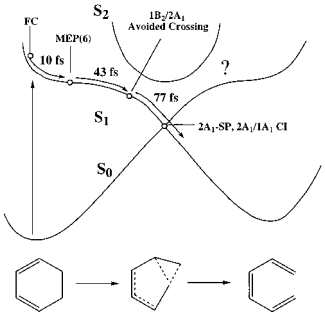

that the reverse reaction (ie. the photoinduced ring closure of hexatriene) occurs with the same type of mechanism (denoted by "?"). The mechanism of this reaction will be the subject of future work.

One important feature of the mechanism proposed above is that, despite the extreme speed of this reaction, it features a multimode reaction coordinate. Accordingly, the photoexcited reactant structure (CHD) is not directly accelerated toward the hexatriene product structure but initially evolves along totally symmetric modes. A multimode coordinate seems to be a common feature of a number of ultrafast reactions such as in linear conjugated hydrocarbons,[5] protonated Schiff bases,[39] and cyanine dyes.[40] This same type of coordinate has been previously proposed, on the basis of Resonance Raman spectra analysis, for the ring-opening of cyclooctatriene to octatetraene.[41] In this case the initial relaxation involved a ring flattening rather than an out-of-plane deformation.

The ultrafast reaction "mechanism" suggested above is based mainly on the evaluation of steepest descent paths and, more generally, on the shape of the potential energy surfaces. This analysis provides a "static" view of the reaction, and the actual dynamics can only be inferred by considering the possible effects of accumulated momentum; that is, we compute static properties of the potential energy surfaces and—qualitatively—evaluate dynamic effects. Although the pathway changes direction several times, it remains in our model a one-dimensional line in *f*-dimensional space. To some extent, this is an oversimplification. However, intramolecular vibrational relaxation (IVR) can be estimated to take place in the range 0.1−1 ps (as in dye molecules[42]); it redistributes kinetic energy, released along the reaction path, to other modes. Thus, IVR initially only plays the role of a heat bath, damping recurrences and coherent oscillations. (Such questions have previously been addressed for butadiene, the chromophore of cyclohexadiene.[43]) Even in this case, the minimum energy path is still the "guide line" for the molecule. Only after a multiple of the IVR time constants (for reactions which are slower, e.g., due to a barrier), would statistical and equilibrium considerations come into play.

Appendix: Minimum Energy Path Computation along the (f − 2)-Dimensional Intersection Space.

The existence of a continuous set of CI funnels is a mere consequence of the fact that the optimized $2A_1/1A_1$ CI is only a single point (actually an energy minimum) within an extended (f − 2)-dimensional intersection space (where f is the number of vibrational degrees of freedom of the molecule).

An IRD search entails the location of an energy minimum, **P′**, within an (f − 1)-dimensional spherical cross-section centered on the initial point, **P** (the "pivot point"). The vector connecting **P** with **P′** defines a steepest descent direction at the pivot point **P**. The basic idea of the new method proposed here

SCHEME 2

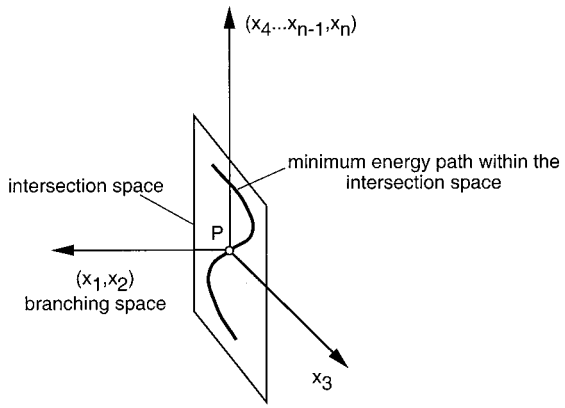

is to perform an IRD search with the additional constraint that both points **P** and **P′** must belong to an intersection space. This space is an ($f - 2$)-dimensional set of conical intersection points where the upper and lower states are degenerate.

At a conical intersection point **P** between two electronic states, one can always distinguish two directions $\mathbf{x_1}$ and $\mathbf{x_2}$ which define the branching space. For $\mathbf{x_1}$ and $\mathbf{x_2}$, one can choose the gradient difference (GD) and the nonadiabatic coupling (NADC) vectors of the two intersecting electronic states. A deformation of the molecular structure within this plane lifts the degeneracy of the two states. Thus, the ($f - 2$)-dimensional intersection space can be visualized as a plane in a three-dimensional diagram centered on **P**, where the branching space is represented by one axis and the other two axes correspond to two subsets of all the other orthogonal axes (eg. $\mathbf{x_3}$ and ($\mathbf{x_4}$, ..., $\mathbf{x}_n$)). In this representation the intersection space will appear as a surface (see Scheme 2). If, in the same diagram, we plot the excited-state energy as a contour on a spherical cross section of radius **r** *centered on P*, the intersection of the two potential energy surfaces will appear as shown in Figure 10a. The intersection space (see plane in Scheme 2) will intersect the spherical cross section along a circle, and along this circle one can distinguish one or more energy minima. We call these minima **P′**, **P″** etc. The vectors **PP′**, **PP″**, etc., then define at **P** directions of steepest descent within the intersection space.

Taking the point **p** on the sphere as the starting point of the search for **P′**, we define at **p** the quantity $\mathbf{g_{tot}}$ as

$$\mathbf{g_{tot}} = \mathbf{g} + \mathbf{f}$$

with

$$\mathbf{g} = (\partial E_2/\partial \mathbf{x}_3, \partial E_2/\partial \mathbf{x}_4, ..., \partial E_2/\partial \mathbf{x}_n) \quad (1)$$

and

$$\mathbf{f} = 2(E_2 - E_1)\mathbf{x_1}/(\mathbf{x_1} \cdot \mathbf{x_1})^{1/2} \quad (2)$$

where E_2 and E_1 are the energies of the upper and lower states, respectively. A minimum in the ($f - 2$)-dimensional intersection space satisfies the relationship $\mathbf{g_{tot}} = 0$. In our procedure, we look for conical intersection points **P′** which satisfy the analogous relationship:

$$\mathbf{Hg_{tot}} = \mathbf{Hg} + \mathbf{Hf} = 0$$

where **Hg** and **Hf** are the respective projections of the vectors **g** and **f** onto the plane tangent to the hypersphere at point **p** (see Figure 10b). On the basis of the above relationship, a new point **q** is predicted that lies on the tangent plane α, but not on the hypersphere surface. Thus, we define **p′** as the predicted point, which is the projection on the hypersphere surface of **q**. This procedure is iterated until $\mathbf{Hg_{tot}}$ satisfies the default *Gaussian 94* convergence thresholds. At this point we set **P′** = **p′**.

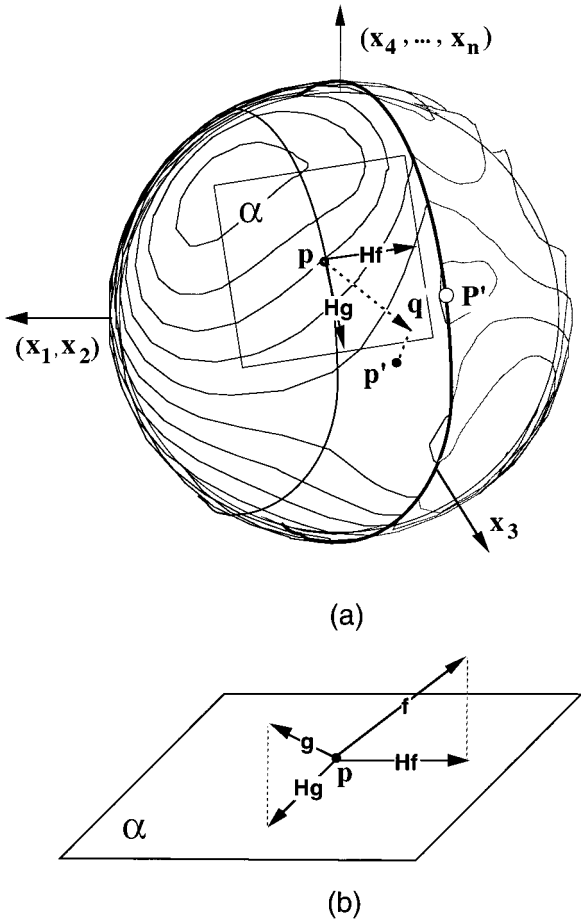

Figure 10. (a) Hyperspherical cross section of the *f*-dimensional PES. The sphere is centered on a point **P** (not shown) in the ($f - 2$)-dimensional intersection space; the latter is represented by a plane spanned by $\mathbf{x_3}$ and ($\mathbf{x_4}$, ..., $\mathbf{x}_n$). (b) Projection of the **g** and **f** vectors on the tangent plane α.

A full steepest descent line starting at **P** can then be generated by moving the pivot point position to the new optimized point **P′** and repeating the procedure.

In practice, the vectors **g** and **f** are evaluated using the CIO procedure available in *Gaussian 94*. The radius of the hypersphere is usually chosen to be small (typically about 0.25−0.5 units in mass-weighted Cartesians) in order to locate the steepest direction in the vicinity of the starting point **P** (the center of the hypersphere). The method used for finding the energy minimum on the hyperspherical cross section of the intersection space (see Figure 10) is the one implemented in the IRD method mentioned above,[15a] which uses mass-weighted Cartesians. We just replace the original gradient with the $\mathbf{Hg_{tot}}$ gradient defined above.

In summary, the optimization process described above locates a *steepest descent line in mass-weighted Cartesians within the intersection space* using the IRD vector to define the direction to follow.

Acknowledgment. Funding has been provided by the Università degli Studi di Siena (Fondi per Progetto di Ateneo

A.A. 1999/2000) and NATO (CRG 950748). C.S.P. gratefully acknowledges the award of an EU Marie Curie Research Fellowship (HPMF-CT-199900384).

References and Notes

(1) van der Lugt, W. T. A. M.; Oosterhoff, L. J. *J. Am. Chem. Soc.* **1969**, *91*, 6042.

(2) Klessinger, M.; Michl, J. *Excited States and Photochemistry of Organic Molecules*; VCH: New York, 1995.

(3) Bernardi, F.; Olivucci, M.; Robb, M. A. *Chem. Soc. Rev.* **1996**, *25*, 321.

(4) Celani, P.; Ottani, S.; Olivucci, M.; Bernardi, F.; Robb, M. A. *J. Am. Chem. Soc.* **1994**, *116*, 10141.

(5) (a) Garavelli, M.; Bernardi, F.; Olivucci, M.; Vreven, T.; Klein, S.; Celani, P.; Robb, M. A. *Faraday Discuss.* **1998**, *110*, 51. (b) Garavelli, M.; Celani, P.; Bernardi, F.; Robb, M. A.; Olivucci, M. *J. Am. Chem. Soc.* **1997**, *119*, 11487.

(6) Celani, P.; Bernardi, F.; Robb, M. A.; Olivucci, M. *J. Phys. Chem.* **1996**, *100*, 19364.

(7) Klessinger, M. *Angew. Chem., Int. Ed. Engl.* **1995**, *34*, 549.

(8) Trushin, S. A.; Fuss, W.; Schikarski, T.; Schmid, W. E.; Kompa, K. L. *J. Chem. Phys.* **1997**, *106*, 9386.

(9) Fuss, W.; Schmid, W. E.; Trushin, S. A. *J. Chem. Phys.* 2000, *112*, 8347.

(10) Frisch, M. J.; Trucks, G. W.; Schlegel, H. B.; Gill, P. M. W.; Johnson, B. G.; Robb, M. A.; Cheeseman, J. R.; Keith, T.; Peterson, G. A.; Montgomery, J. A.; Raghavachari, K.; Al-Laham, M. A.; Zakrzewski, V. G.; Ortitz, J. V.; Foresman, J. B.; Peng, C. Y.; Ayala, P. Y.; Chen, W.; Wong, M. W.; Andres, J. L.; Replogle, E. S.; Gomperts, R.; Martin, R. L.; Fox, D. J.; Binkley, J. S.; Defrees, D. J.; Baker, J.; Stewart, J. J. P.; Head-Gordon, M.; Gonzalez, C.; Pople, J. A. *Gaussian 94*, Revision B.2; Gaussian, Inc.: Pittsburgh, PA, 1995.

(11) (a) Andersson, K.; Malmqvist, P.-Å.; Roos, B. O. *J. Chem. Phys.* **1992**, *96*, 1218. (b) Finley, J. Malmqvist, P.-Å. Roos, B. O.; Serrano-Andrés, L. *Chem. Phys. Lett.* **1998**, *288*, 299.

(12) Andersson, K.; Blomberg, M. R. A.; Fülscher, M. P.; Karlström, G.; Lindh, R.; Malmqvist, P.-Å.; Neogrády, P.; Olsen, J.; Roos, B. O.; Sadlej, A. J.; Schütz, M.; Seijo, L.; Serrano-Andrés, L.; Siegbahn, P. E. M.; Widmark, P.-O. *MOLCAS*, Version 4; Lund University: Sweden, 1997.

(13) Miller, W. H.; Handy, N. C.; Adams, J. E. *J. Chem. Phys.* **1980**, *72*, 99.

(14) Truhlar, D. G.; Gordon, M. S. *Science* **1990**, *249*, 491.

(15) (a) Celani, O.; Robb, M. A.; Garavelli, M.: Bernardi, F.; Olivucci, M. *Chem. Phys. Lett.* **1995**, *243*, 1. (b) Bearpark, M. J.; Robb, M. A.; Schlegel, H. B. *Chem. Phys. Lett.* **1994**, *223*, 269.

(16) Fuss, W.; Schmid, W. E.; Trushin, ISRAPS Bulletin **2000**, *11*, 7.

(17) Minnaard, N. G.; Havinga, E. *Recueil* **1973**, *92*, 1179.

(18) McDiarmid, R.; Sabliæ, A.; Doering, J. P. *J. Chem. Phys.* **1985**, *83*, 2147.

(19) Warshel, A. M.; Karplus, M. *Chem. Phys. Lett.* **1972**, *17*, 7.

(20) O'Connor, R.; Goldblatt, L. A. *Anal. Chem.* **1954**, *26*, 1726.

(21) Fuss, W.; Schikarski, T.; Schmid, W. E.; Trushin, S.; Kompa, K. L.; Hering, P. *J. Chem. Phys.* 1997, *106*, 2205.

(22) Merchán, M.; Serrano-Andrés, L.; Slater, L. S.; Roos, B. O.; McDiarmid, R.; Xing, X. *J. Phys. Chem. A* **1999**, *103*, 5468.

(23) Kimura, K.; Katsumata, S.; Achiba, Y.; Yamazaki, T.; Iwata, S. In *Handbook of HeI Photoelectron Spectra of Fundamental Organic Molecules*; Japan Scientific Society Press: Tokyo, 1981.

(24) Sablić, A.; Güsten, H. *Atmos. Environ.* **1990**, *24*, 73.

(25) Fuss, W.; Hering, P.; Kompa, K. L.; Lochbrunner, S.; Schikarski, T.; Schmid, W. E.; Trushin, S. A. *Ber. Bunsen-Ges. Phys. Chem.* **1997**, *101*, 500.

(26) Reid, P. J.; Doig, S. J.; Mathies, R. A. *J. Phys. Chem.* **1990**, *94*, 8396.

(27) Reid, P. J.; Doig, S. J.; Wickham, S. D.; Mathies, R. A. *J. Am. Chem. Soc.* **1993**, *115*, 4754.

(28) Ohta, K.; Naitoh, Y.; Saitow, K.; Tominaga, K.; Hirota, N.; Yoshihara, K. *Chem. Phys. Lett.* **1996**, *256*, 629.

(29) Ohta, K.; Naitoh, Y.; Tominaga, K.; Hirota, N.; Yoshihara, K. *J. Phys. Chem. A* **1998**, *102*, 35.

(30) Hofmann, A.; de Vivie-Riedle, R. *J. Chem. Phys.* 2000, *112*, 5054.

(31) Hudson, B. S.; Kohler, B. E.; Schulten, K. In *Excited States;* Lim, E. C., Ed.; Academic Press: New York, 1982; p 1.

(32) Ye, T.; Gershgoren, E.; Friedman, N.; Ottolenghi, M.; Sheves, M.; Ruhman, S. *Chem. Phys. Lett.* **1999**, *314*, 429.

(33) Lawless, M. K.; Wickham, S. D.; Mathies, R. A. *Acc. Chem. Res.* **1995**, *28*, 493.

(34) Trushin, S. A.; Diemer, S.; Fuss, W.; Kompa, K. L.; Schmid, W. E. *Phys. Chem. Chem. Phys.* **1999**, *1*, 1431.

(35) Baldwin, J. E.; Krueger, S. M. *J. Am. Chem. Soc.* **1969**, *91*, 6444.

(36) Laarhoven, W. H.; Jacobs, H. J. C. in *Organic Photochemistry and Photobiology*, Horspool, W. M., Song, P.-S., Eds.; CRC Press: Boca Raton, 1995; p 143.

(37) Pullen, S. H.; Anderson, N. A.; Walker, L. A., II; Sension, R. J. *J. Chem. Phys.* **1998**, *108*, 556.

(38) Fuss, W.; Lochbrunner, S. S.; Müller, A. M.; Schikarski, T.; Schmid, W. E.; Trushin, S. A. *Chem. Phys.* **1998**, *232*, 161.

(39) Gonzalez-Luque, R.; Garavelli, M.; Bernardi, F.; Merchan, M.; Robb, M. A.; Olivucci, M. *Proc. Nat. Acad. Sci. U.S.A.* **2000**, *97*, 9379−9384.

(40) Sanchez-Galvez, A.; Hunt, P.; Robb, M. A.; Olivucci, M.; Vreven, T.; Schlegel, H. B. *J. Am. Chem. Soc.* **2000** 112, 2911−2924.

(41) Lawless, M. K.; Wickham, S. D.; Mathies, R. A. *Acc. Chem. Res.* **1995**, *28*, 493−502.

(42) Elsässer, T.; Kaiser, W. *Annu. Rev. Phys. Chem.* **1991**, *42*, 83.

(43) Krawczyk, R. P.; Malsch, K.; Hohlneicher, G.; Gillen, R. C.; Domcke, W. *Chem. Phys. Lett.* **2000**, *320*, 535.